# Supporting Information

Hyeon *et al.* 10.1073/pnas.0813266106

## SI Text

**Importance of Side-Chain Interaction.** A comparison between the open (PDB ID code 1CMK) and closed (PDB ID code 1ATP) forms of PKA suggests that the side chains play important roles in the PKA compaction (1). For instance, (*i*) when measured by using the closest phosphate oxygen of phosphorylated Thr-197 (P-Thr-197) to the N2 atom of His-87, the distance between P-Thr-197 and His-87 reduces from 7.1 to 2.8 Å (2), whereas, the distance between the 2 $C_\alpha$ atoms of P-Thr-197 and His-87 only changes from 11.4 to 10.4 Å. During the transition of PKA from open to closed form, P-Thr-197 and His-87 can make a hydrogen bond simply by changing the orientation of side chains. (*ii*) The association between the side chain of Phe-327 and the adenine of ATP, whose distance is 3.4 Å in the closed form, is important for the stabilization of C-terminal tail (3). The side chain of Phe-327 protruding out of the backbone of the C-terminal tail can enhance the specificity of contact formation with ATP. A $C_\alpha$-backbone model with uniform interactions lacks such a feature. (*iii*) The side chains of charged residues (Lys, Arg) and hydrophobic and bulky residues (Phe, Tyr, Trp) are used to recognize the phosphate/ribose groups and adenine ring of ATP, respectively (see Fig. S1*B*). Thus, a number of important features associated with the conformational transition of PKA are involved with side-chain dynamics. To introduce side chains into a coarse-grained model, we have modified the $C_\alpha$ (or single bead) -based self-organized polymer (SOP) model that had successfully been used in the recent studies on various proteins (4) and molecular motors (5) (see below for details). Because many side-chain interactions in PKA are involved between charged residues (Asp, Glu, Lys, His, Arg) or in hydrophobic residues (Phe, Tyr, Trp), we have restricted side chains to 8 types of residues (see Fig. S4) and 2 phosphorylated residues, P-Thr-197 and P-Ser-338. The interaction centers of side chains are modeled by using, instead of center of mass, the most distant heavy atom (N, C, O, or P) from the $C_\alpha$ backbone in the crystal structure, so that the contacts between bulky side chain can be included by using $R_c^S$ = 5-Å cutoff criteria for side-chain contacts (see below). We did not include smaller side chains, such as Met, Leu, Gln, and others, in the model so as to minimize the computational cost. Including other smaller side chains into the model should not qualitatively change the dynamics.

**Energy Hamiltonian.** The full energy potential associated with the transition dynamics of PKA is divided into 3 parts; the energy Hamiltonians for PKA ($H^{\mathrm{PKA}}$), ATP ($H^{\mathrm{ATP}}$), and interactions between PKA and ATP ($H^{\mathrm{ATP-PKA}}$). The energy Hamiltonian and its parameters for PKA are based on the previous SOP model for proteins (6). But here, the energy Hamiltonian has additional terms for side chains ($S$). The full Hamiltonian is given by $H_{\mathrm{full}} = H^{\mathrm{PKA}} + H^{\mathrm{ATP}} + H^{\mathrm{ATP-PKA}} = H^{(\mathrm{O})}_{\mathrm{FENE}} + H^{\mathrm{BB(O)}}_{\mathrm{NON}} + H^{\mathrm{SS(O)}}_{\mathrm{NON}} + H^{\mathrm{BS(O)}}_{\mathrm{NON}} + H^{\mathrm{BB(C\cap O_c)}}_{\mathrm{NON}} + H^{\mathrm{SS(C\cap O_c)}}_{\mathrm{NON}} + H^{\mathrm{ATP}}_{\mathrm{FENE}} + H^{\mathrm{ATP-BS(C)}}_{\mathrm{NON}}$, where the Hamiltonian for PKA ($H^{\mathrm{PKA}}$) is divided into the contributions from backbone connectivity and noncovalent bonds between backbone–backbone (BB), side chain–side chain (SS), and backbone–side chain (BS). $H^{\mathrm{ATP}}$ models the ATP molecule as a collection of harmonically constrained heavy atoms (C, N, O, and P), and $H^{\mathrm{ATP-BS(C)}}_{\mathrm{NON}}$ defines the interaction between ATP and PKA.

***Connectivity of the backbone and BS.*** The finite extensible nonlinear elastic (FENE) potential is used to model the connectivity along the backbone ($B_iB_{i+1}$ with $i$ = 1,2,… $N_B$ − 1) and between the backbone and side chain ($B_iS_i$ where $i$ = 1,2, … $N_S$).

$$H^{(O)}_{FENE} = \sum_{i=1}^{N_B-1}\left( -\frac{k}{2}R_o^2\log\left[ 1 - \frac{(r_{B_iB_{i+1}} - r^O_{B_iB_{i+1}})^2}{R_o^2}\right]\right) + \sum_{i=1}^{N_S}\left( -\frac{k}{2}R_o^2\log\left[ 1 - \frac{(r_{B_iS_i} - r^O_{B_iS_i})^2}{R_o^2}\right]\right), \quad \textbf{[s1]}$$

where $k$ = 20 kcal/(mol ×Å$^2$), $R_o$ = 2 Å, and the superscript in $r^{\mathrm{O}}_{BiBi+1}$ and $r^{\mathrm{O}}_{BiSi}$ denotes that the equilibrium distance between 2 neighboring interaction sites is defined from the open (O) structure.

***Noncovalent interactions stabilizing the open structure.*** The noncovalent interactions between the BB, the SS, and the BS that stabilize the open structure are modeled by using Lennard–Jones potentials as follows.

$$H^{BB(O)}_{NON} = \sum_{i=1}^{N_{B-3}}\sum_{j=i+3}^{N_B}\varepsilon_h(B_i,B_j)\left[\left(\frac{r^O_{B_iB_j}}{r_{B_iB_j}}\right)^{12} - 2\left(\frac{r^O_{B_iB_j}}{r_{B_iBj}}\right)^{6}\right]\Delta^O_{B_iB_j} + \sum_{i=1}^{N_B-2}\varepsilon_l\left(\frac{\sigma}{r_{B_iB_{i+2}}}\right)^6 + \sum_{i=1}^{N_B-3}\sum_{j=i+3}^{N_B}\varepsilon_l\left(\frac{\sigma}{r_{B_iB_j}}\right)^6(1-\Delta^O_{B_iB_j}), \quad \textbf{[s2]}$$

$$H^{SS(O)}_{NON} = \sum_{i=1}^{N_S-1}\sum_{j=i+1}^{N_S}\left\{\varepsilon_h(S_i,S_j)\left[\left(\frac{r^O_{S_iS_j}}{r_{S_iS_j}}\right)^{12} - 2\left(\frac{r^O_{S_iS_j}}{r_{S_iS_j}}\right)^{6}\right]\Delta^O_{S_iS_j} + \varepsilon_l\left(\frac{\sigma}{r_{S_iS_j}}\right)^6(1-\Delta^O_{S_iS_j})\right\}, \quad \textbf{[s3]}$$

and

$$H^{BS(O)}_{NON} = \sum_{i=1}^{N_B}\sum_{j=1}^{N_S}\left\{\varepsilon_h(B_i,S_j)\left[\left(\frac{r^O_{B_iS_j}}{r_{B_iS_j}}\right)^{12} - 2\left(\frac{r^O_{B_iS_j}}{r_{B_iS_j}}\right)^{6}\right]\Delta^O_{B_iS_j} + \varepsilon_l\left(\frac{\sigma}{r_{B_iS_j}}\right)^6(1-\Delta^O_{B_iS_j})\right\}. \quad \textbf{[s4]}$$

To implement Go-like interactions, we set $\Delta^{\mathrm{O}}_{B_iB_j}$, $\Delta^{\mathrm{O}}_{B_iS_j}$ = 1 if the distance between the 2 interaction centers in the open structure is $<R_c^B$ = 8 Å, otherwise $\Delta^{\mathrm{O}}_{B_iB_j}$, $\Delta^{\mathrm{O}}_{B_iS_j}$ = 0. For the SS interaction, we defined the cutoff distance for the contact as $R_c^S$ = 5 Å. For the pairs satisfying $\Delta^{\mathrm{O}}_{X_iY_j}$ = 1, the distance that minimizes the above Lennard–Jones potential is taken from the open structure. The strength of the nonbonded interaction is controlled by $\varepsilon_h(X_i,Y_j)$ where $\varepsilon_h(B_i,B_j) = \varepsilon_h(S_i,S_j) = \varepsilon_h(B_i,S_j)$ = 1 kcal/mol. For the parameters for repulsive potentials, $\varepsilon_l$= 1 kcal/mol and $\sigma$ = 3.8 Å are chosen. The parameter $\varepsilon_h$ for single-bead SOP model for proteins is $\varepsilon_h$ =

1–2 kcal/mol. For the SOP model with side chains, assigning $\varepsilon_h$ = 1 kcal/mol for backbone and side chain, respectively, is similar to delocalizing the interaction to the backbone and side chain.

***Noncovalent interactions stabilizing the closed structure.*** The perturbative interactions to the open energy Hamiltonian from the contacts stabilizing the closed structure are included as

$$H_{NON}^{BB(C\cap O^C)} = \sum_{i=1}^{N_B-3}\sum_{j=i+3}^{N_B}\varepsilon_h(B_i,B_j)\left[\left(\frac{r_{B_iB_j}^{\{C\cap O^c\}}}{r_{B_iB_j}}\right)^{12} - 2\left(\frac{r_{B_iB_j}^{\{C\cap O^c\}}}{r_{B_iB_j}}\right)^{6}\right]\Delta_{B_iB_j}^{\{C\cap O^c\}} \qquad \textbf{[s5]}$$

and

$$H_{NON}^{SS(C\cap O^C)} = \sum_{i=1}^{N_S-1}\sum_{j=i+1}^{N_S}\varepsilon_h(S_i,S_j)\left[\left(\frac{r_{S_iS_j}^{\{C\cap O^c\}}}{r_{S_iS_j}}\right)^{12} - 2\left(\frac{r_{S_iS_j}^{\{C\cap O^c\}}}{r_{S_iS_j}}\right)^{6}\right]\Delta_{S_iS_j}^{\{C\cap O^c\}}. \qquad \textbf{[s6]}$$

The notation $\{C\cap O^C\}$denotes the contacts present only in the closed structure. The remaining parameters are identically defined as in $H_{\mathrm{NON}}^{XY(O)}$. The forms of Eqs. **s5** and **s6** from Eqs. **s2–s4** in that the repulsive terms are not included. The excluded volume interaction is already taken into account by the open structure.

**Modeling the ATP molecule.** The ATP molecule is modeled as a collection of heavy atoms (C, N, O, and P) harmonically constrained as

$$H_{FENE}^{ATP} = \sum_{i=1}^{N_{\mathrm{ATP}}-1}\sum_{j=i+1}^{N_{\mathrm{ATP}}}\left(-\frac{k}{2}R_o^2\log\left[1-\frac{(r_{A_iA_j}-r_{A_iA_j}^{\mathrm{ATP}})^2}{R_o^2}\right]\right), \qquad \textbf{[s7]}$$

where $k$ = 20 kcal/(mol ×Å$^2$) and $R_o$ = 2 Å. $N_{\mathrm{ATP}}$ is the number of total heavy atoms consisting the ATP molecule.

**ATP-PKA interaction.** Last, we model the interaction between the ATP and PKA by using

$$H_{NON}^{ATP-BS(C)} = \sum_{i=1}^{N_A}\sum_{j=1}^{N_B}\left\{\varepsilon_h(A_i,B_j)\left[\left(\frac{r_{A_iB_j}^{C}}{r_{A_iB_j}}\right)^{12} - 2\left(\frac{r_{A_iB_j}^{C}}{r_{A_iB_j}}\right)^{6}\right]\Delta_{A_iB_j}^{C} + \varepsilon_l^{ATP}\left(\frac{\sigma}{r_{A_iB_j}}\right)^6(1-\Delta_{A_iB_j}^{C})\right\} + \sum_{i=1}^{N_A}\sum_{j=1}^{N_S}\left\{\varepsilon_h(A_i,S_j)\left[\left(\frac{r_{A_iS_j}^{C}}{r_{A_iS_j}}\right)^{12} - 2\left(\frac{r_{A_iS_j}^{C}}{r_{A_iS_j}}\right)^{6}\right]\Delta_{A_iS_j}^{C} + \varepsilon_l^{ATP}\left(\frac{\sigma}{r_{A_iS_j}}\right)^6(1-\Delta_{A_iS_j}^{C})\right\} \qquad \textbf{[s8]}$$

where we assign $\varepsilon_h(A_i,B_j) = \varepsilon_h(A_i,S_j)$ = 0.2 kcal/mol and $\varepsilon_l^{\mathrm{ATP}}$ = 0.1 kcal/mol and cutoff distance to define $\Delta_{A_iB_j}^{C}$, $\Delta_{A_iS_j}^{C}$ is set 8 Å. The reason for using small values for $\varepsilon_h$ and $\varepsilon_l$ is that we represent the ATP molecule by using the individual heavy atoms. As long as the ATP molecule can bind and stay in its binding site, the PKA undergoes the conformational change from the open to reach the closed structure.

**Simulations.** To perform simulations with a realistic friction coefficient, the simulations under overdamped condition are performed by using the Brownian dynamics algorithm (10, 11)

$$\vec{r}_i(t+\Delta t) = \vec{r}_i(t) - \zeta_H^{-1}\vec{\nabla}_{\vec{r}}H(\{\vec{r}\})\times\Delta t + \vec{R}(t) \qquad \textbf{[s9]}$$

with $\langle R_\alpha(t)R_\beta(t')\rangle = 2k_BT;\zeta_H^{-1}\Delta t\delta(t-t')\delta_{\alpha\beta}$. The natural measure for the time for overdamped condition at a simulation temperature $T_s$ is $\tau_H \approx \zeta_H a^2/k_BT_s = [(\zeta_H\tau_L/m)\varepsilon_h/k_BT_s]\times\tau_L$, where $m$, $a$, and $\varepsilon_h$ are, respectively, the mass, size, and energy scale of interaction of the coarse-grained bead, from which the characteristic time is estimated as $\tau_L = (ma^2/\varepsilon_h)^{1/2} \approx 3$ ps. If we set $\zeta_H$ (= $6\pi\eta a$) ≈ 50 $m/\tau_L$, which can be calculated by using water viscosity ($\eta \approx 1$ $cP$) and the size of the coarse-grained center ($a \approx 3.8$ Å), and choose an integration time step of $\Delta t$ = 0.02 $\tau_H$, then $10^6$ simulation steps at $T_s$ = 310 K ($k_BT_s \approx 0.6$ kcal/mol) correspond to 5 $\mu$s in real time ($10^6\times\Delta t = 5$ $\mu$s). For the ATP molecule modeled in atomic representation, we set $\zeta_H^{\mathrm{ATP}} = 10\ m/\tau_L$ and solved the equation of motion.

**Effect of Closed Contacts on the PKA Dynamics.** As mentioned in the main text, the pure closed contacts ($C\cap O^C$, see Fig. 2*B*) serve as additional contributions to the PKA–ATP interactions. We have tested the efficacy of a system Hamiltonian ($H_{\mathrm{closed}}^{\mathrm{w/o}}$), which excludes the closed contacts, in driving the open-to-closed transition. Under $H_{\mathrm{closed}}^{\mathrm{w/o}}$ energy Hamiltonian [$H_{\mathrm{closed}}^{\mathrm{w/o}} = H_{\mathrm{FENE}}^{(O)} + H_{\mathrm{NON}}^{\mathrm{BB(O)}} + H_{\mathrm{NON}}^{\mathrm{SS(O)}} + H_{\mathrm{NON}}^{\mathrm{BS(O)}} + H_{\mathrm{FENE}}^{\mathrm{ATP}} + H_{\mathrm{NON}}^{\mathrm{ATP\text{-}BS(C)}}$], i.e., without closed contacts, PKA can make transitions toward the closed structure to a reasonable amount although the transition is not as complete as the one under $H_{\mathrm{full}}$. The cartoon in Fig. 1*B* succinctly illustrates the induced fit mechanism and the effect of the pure closed contacts on the PKA compaction. The consequence of dynamics under $H_{\mathrm{closed}}^{\mathrm{w/o}}$ are shown and compared with that under $H_{\mathrm{full}}$ in Figs. 2*D* and 3*C*.


1. Johnson DA, Akamine P, Radzio-Andzeim E, Madhusudan, Taylor SS (2001) Dynamics of cAMP-dependent protein kinase. *Chem Rev* 101:2243–2270.
2. Kornev AP, Taylor SS, Ten Eyck LF (2008) A generalized allosteric mechanism for *cis*-regulated cyclic nucleotide binding domains. *PLoS Comp Biol* 4:1–9.
3. Andersen MD, Shaffer J, Jennings PA, Adams JA (2001) Structural characterization of protein kinase A as a function of nucleotide binding-hydrogen–deuterium exchange studies using matrix-assisted laser desorption ionization-time of flight mass spectrometry detection. *J Biol Chem* 276:14204–14211.
4. Hyeon C, Lorimer GH, Thirumalai D (2006) Dynamics of allosteric transition in GroEL. *Proc Natl Acad Sci USA* 103:18939–18944.
5. Chen J, Dima RI, Thirumalai D (2007) Allosteric communication in dihydrofolate reductase: Signaling network and pathways for closed to occluded transition and back. *J Mol Biol* 374:250–266.
6. Hyeon C, Dima RI, Thirumalai D (2006) Pathways and kinetic barriers in mechanical unfolding and refolding of RNA and proteins. *Structure (London)* 14:1633–1645.
7. Hyeon C, Thirumalai D (2007) Mechanical unfolding of RNA: From hairpins to structures with internal multiloops. *Biophys J* 92:731–743.
8. Hyeon C, Onuchic JN (2007) Internal strain regulates the nucleotide binding site of the kinesin leading head. *Proc Natl Acad Sci USA* 104:2175–2180.
9. Hyeon C, Onuchic JN (2007) Mechanical control of the directional stepping dynamics of the kinesin motor. *Proc Natl Acad Sci USA* 104:17382–17387.
10. Ermak DL, McCammon JA (1978) Brownian dynamics with hydrodynamic interactions. *J Chem Phys* 69:1352–1369.
11. Veitshans T, Klimov D, Thirumalai D (1997) Protein folding kinetics: Timescales, pathways and energy landscapes in terms of sequence-dependent properties. *Folding Des* 2:1–22.
12. Black SD, Mould DR (1991) Development of hydrophobicity parameters to analyze proteins which bear post- or cotranslational modifications. *Anal Biochem* 193:72–82.

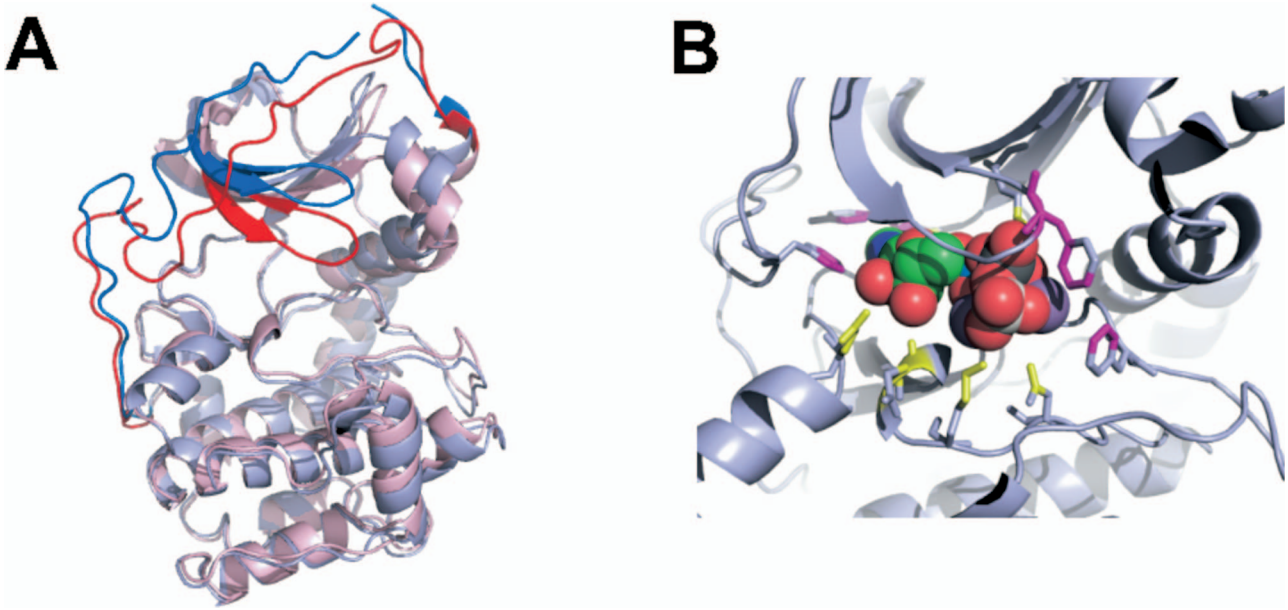


**Fig. S1.** Structures of PKA. (*A*) Open and closed structures are overlapped, showing the differences in glycine-rich loop (residues 47–58) and the C-terminal tail that are colored in bright blue and red for the open and the closed structure, respectively. (B) ATP in the binding pocket. Shown in stick representation are the charged residues (yellow) and hydrophobic and bulky residues (purple) surrounding the ATP.

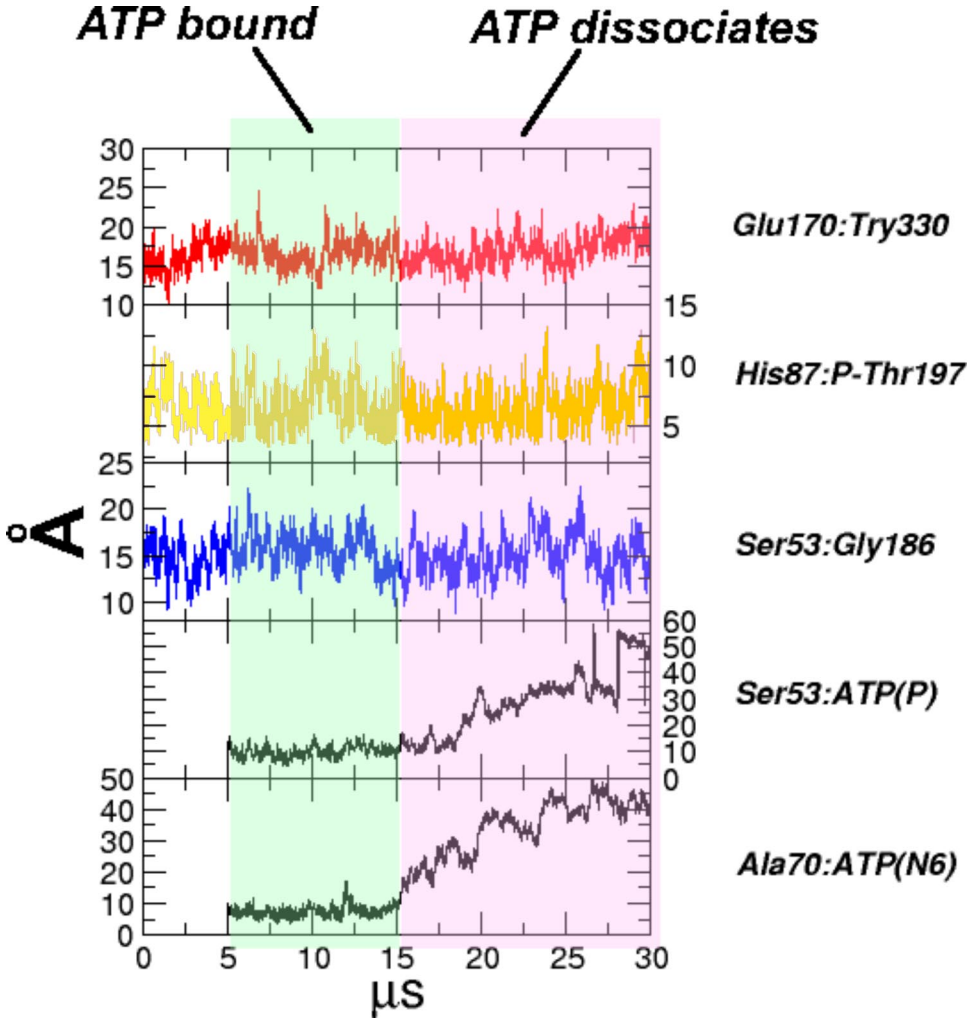


**Fig. S2.** Dynamics of PKA when ATP interactions are weakened by 10-fold. ATP inserted in the binding cleft at 5 $\mu$s eventually dissociates. The shaded regions of the plot show that the ATP inserted to the binding pocket eventually dissociates because of the weakened interaction.

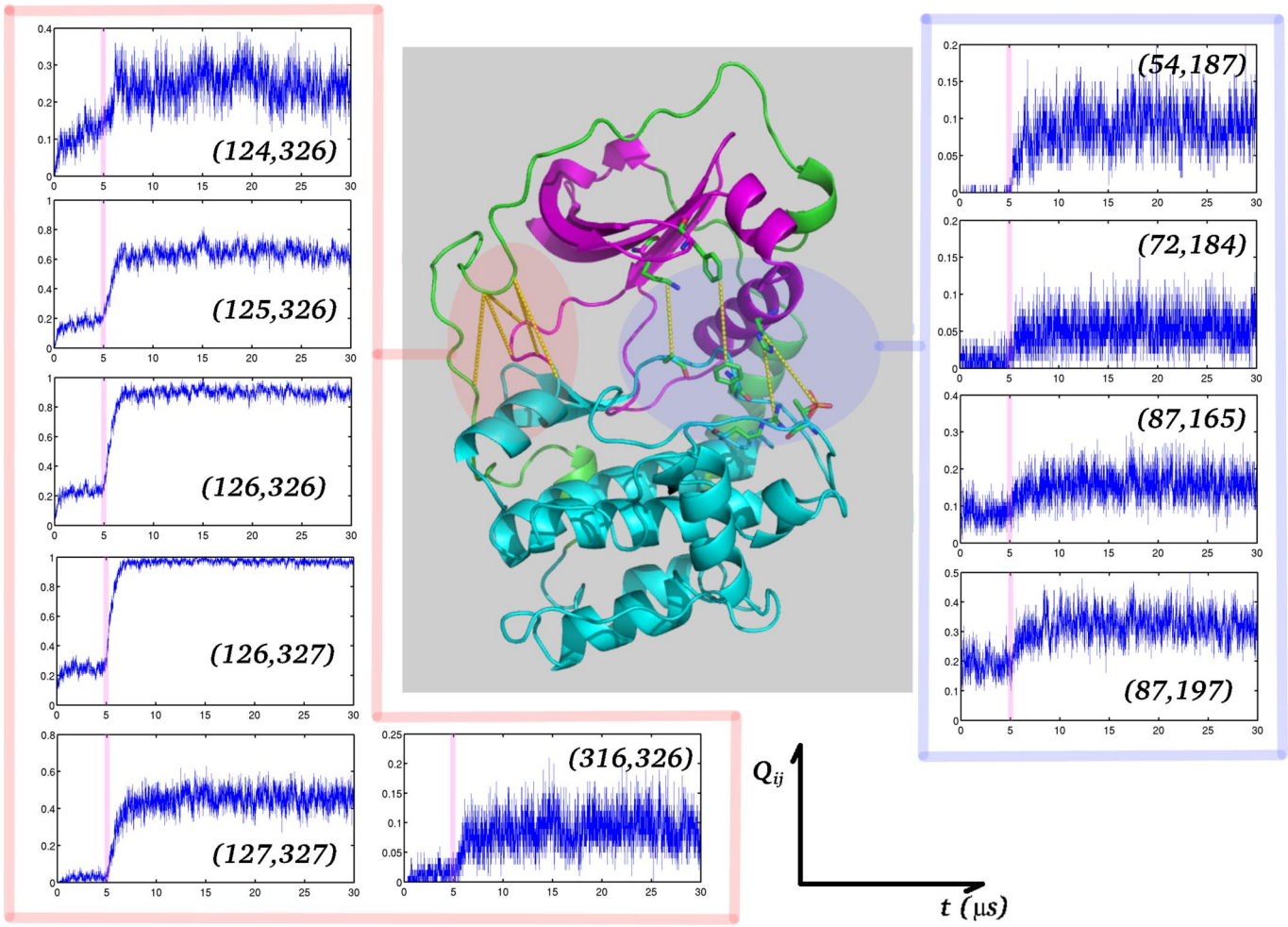


**Fig. S3.** Formations of closed contacts upon ATP binding. Association dynamics of some closed contact pairs are probed by calculating the average fraction of native contacts (Eq. **2**) over 100 trajectories. In the absence of ATP, the native contact pairs from the closed conformation make few contacts, but the contact formations of these pairs are enhanced upon ATP binding. Shown is how the ATP binding enhances the contact formations between the C-terminal tail and the linker (residues 120–127) connecting large and small lobes (region shadowed in pale red), and between the residues in the C-helix and activation loop (region shadowed in pale blue). The yellow lines are the residue pairs whose dynamics are shown in each panel.

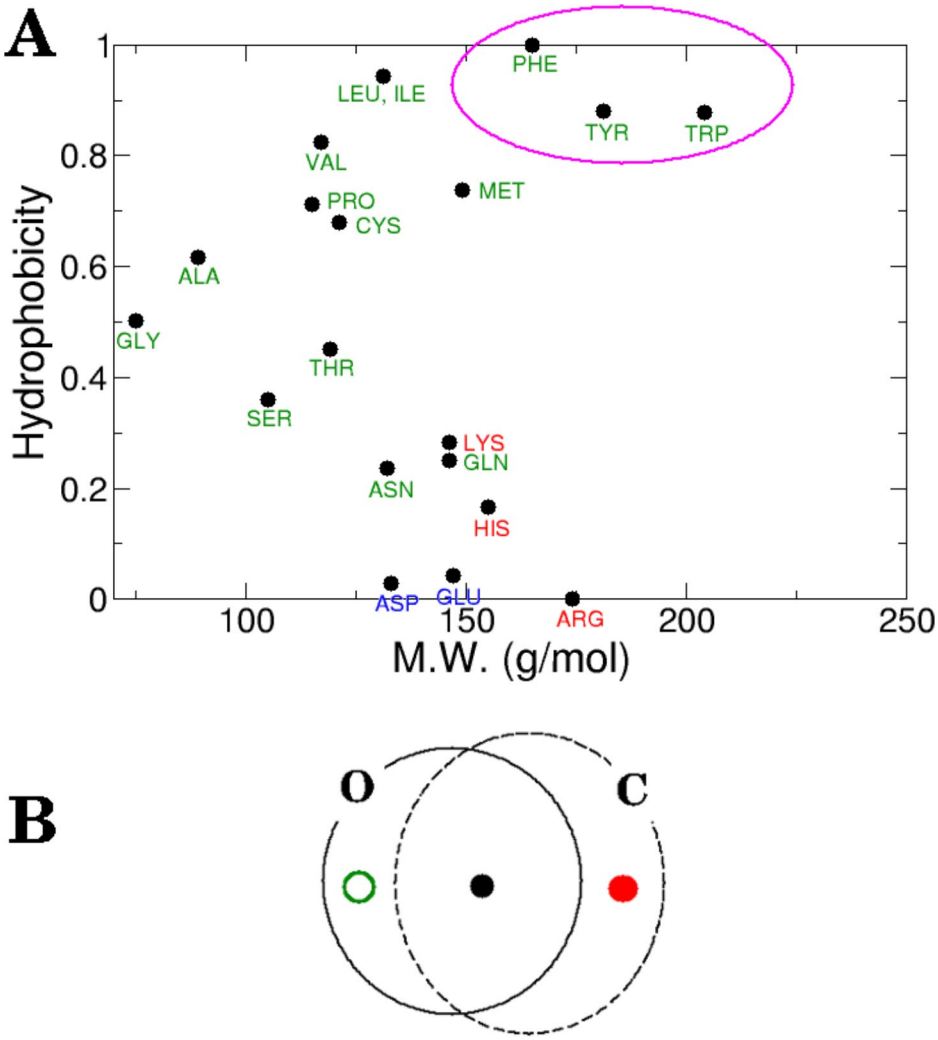


**Fig. S4.** Modeling side chains and native contacts of PKA model. (*A*) Hydrophobicity scale for the 20 amino acids (12). Side chains are modeled explicitly for the bulky/hydrophobic residue (Phe, Tyr, Trp) and for the charged residues (Lys, His, Arg, Asp, Glu). (*B*) Diagram classifying the native contacts from both open and closed structures. The symbol at each area is: the open green circle for the contacts present in open form not absent in closed form ($O \cap C^C$), the filled black circle for the contacts present in both open and closed form ($O \cap C$), and the filled red circle for contacts present only in closed form ($O^C \cap C$). The same symbols are used in the contact maps of Fig. 1 *D* and *E*. The equilibrium contact distances belonging to the filled black circle are taken from those of open structure.

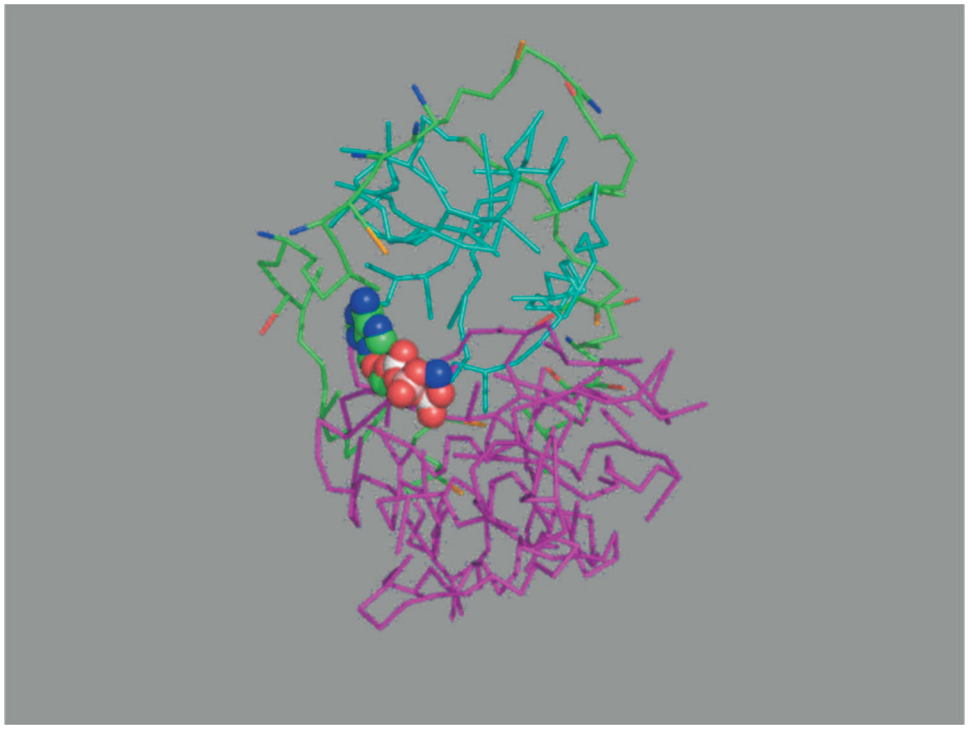

**Movie S1.** A simulation of ATP-binding induced open-to-closed transition of PKA.

Movie S1 (MPG)